# A multi-proxy approach (Ge-Si-Fe, Cr isotopes, Th-U) reveals evidence of oxidative terrestrial weathering in marine chemical sediments from the Neoarchean Temagami BIF, Canada

Michael Bau[1*], Robert Frei[2], Dieter Garbe-Schönberg[3], Sebastian Viehmann[4]

[1] Jacobs University Bremen, Department of Physics and Earth Sciences, Campus Ring 1, 29759 Bremen, Germany.

[2] University of Copenhagen, Department of Geosciences and Natural Resource Management, and Nordic Center for Earth Evolution, Copenhagen 1350, Denmark.

[3] CAU Kiel University, Institute of Geosciences, Ludewig-Meyn-Strasse 10, 24118 Kiel, Germany.

[4] University of Vienna, Department of Lithospheric Research, Althanstr. 14, 1090 Wien, Austria.

**corresponding author (Email: m.bau@jacobs-university.de)*

# A multi-proxy approach (Ge-Si-Fe, Cr isotopes, Th-U) reveals evidence of oxidative terrestrial weathering in marine chemical sediments from the Neoarchean Temagami BIF, Canada

Michael Bau[1*], Robert Frei[2], Dieter Garbe-Schönberg[3], Sebastian Viehmann[4]

## ABSTRACT

Unique deposits that formed in the Precambrian oceans are the Banded Iron-Formations (BIFs) which are chemical sediments comprised of alternating layers of iron- and silica-dominated precipitates. The origin of this enigmatic banding is still debated, with most favoring a primary sedimentary and a few others arguing for a secondary diagenetic origin. We here used a high-resolution integrated multi-proxy approach and report on the Ge-Si-Fe and Th-U systematics and on the isotopic composition of Cr in exceptionally pure adjacent magnetite and metachert bands from the ~2.7 billion years old Temagami BIF, Ontario, Canada. While each of the geochemical proxies alone may still be controversially discussed, our multi-proxy approach sheds new light on their applicability, as the two types of adjacent BIF bands are characterised by distinct geochemical signatures. The magnetite bands show super-crustal (i.e. fractionated) Ge/Si ratios approaching those of modern marine high-temperature hydrothermal fluids, unfractionated Th/U ratios similar to those of crustal rocks, and unfractionated Cr isotope ratios similar to "Bulk Silicate Earth". Adjacent metachert bands, however, show lower (i.e. unfractionated) Ge/Si ratios close to those of modern seawater, river water and crustal rocks, sub-crustal (i.e. fractionated) Th/U ratios and fractionated Cr isotope ratios above those of Bulk Silicate Earth. The composition of the magnetite bands suggests that the original iron-oxyhydroxide precipitated during periods when the Ge, Th, U, and Cr inventory of seawater was dominated by input from mafic crust via anoxic high-temperature hydrothermal fluids. In contrast, the composition of the metachert bands indicates that these formed during times when seawater was dominated by low-temperature riverine input from an evolved landmass that despite its Neoarchean age had provided environments for oxidative Cr and U mobilization during terrestrial weathering. This suggests that habitats with oxygenic photosynthesis may have existed almost 400 million years before the GOE. The systematic difference between the geochemical signature shown by the two types of adjacent BIF bands also demonstrates that the prominent banding of BIFs is a primary depositional feature reflecting precipitation from different watermasses and is not the result of post-depositional separation of an initially homogenous chemical sediment.

## 1. Introduction

Banded Iron-Formations (BIFs) are robust archives for geochemical proxies for the physico-chemical evolution of Early Earth's atmosphere and oceans, provided they are pure, i.e. devoid of detrital aluminosilicates, and pristine, i.e. have remained isochemical systems during diagenesis, metamorphism, hydrothermal overprint and weathering (e.g., Alexander et al., 2009; Bekker et al., 2014; Viehmann et al, 2015). Several studies (Bau and Alexander, 2009; Viehmann et al., 2014; Diekrup et al. 2018; Schulz et al., 2021) demonstrated that the Neoarchean Temagami BIF, Ontario, Canada, provides samples of exceptionally pure and well-preserved marine chemical sediment, allowing to apply and evaluate a set of geochemical proxies used in Early Earth studies.

In this study we use microdrill cores and laser ablation on slabs from the Temagami BIF for an integrated high-resolution investigation of the source proxies Ge-Si-Fe in combination with redox-sensitive Cr isotopes and Th-U relationships to discuss these proxies on the background of published data for the distribution of the rare earths and yttrium (REY) and for Nd and Hf isotopes. The approach of using a combination of geochemical proxies in BIFs, that each individually are controversially discussed, provides a rather straightforward plausability check: If the Ge/Si ratio was indeed a source proxy and fractionated Cr isotopes and Th/U ratios occurred in Archean seawater due to the redox level of the Earth's surface system, they should rather be confined to the metachert bands of Archean BIFs, as these formed from waters that based on their low Ge/Si ratios are assumed to carry terrigenous signals. However, Cr isotopes and

Th/U ratios of the iron-rich bands should usually not be fractionated, because their high Ge/Si ratios are assumed to suggest that they carry mantle signals and formed from seawater affected by anoxic high-temperature hydrothermal fluids that had altered seafloor basalts. Preservation of different geochemical proxy signals in adjacent metachert and magnetite bands should also help to end the longstanding debate whether the prominent banding of BIFs is a depositional feature reflecting precipitation from different water masses, or whether it was produced from an initially homogenous Fe-Si precipitate (e.g., Krapez et al., 2003; Alibert and Kinsley, 2016) during diagenesis or metamorphism, i.e. *after* deposition.

## 2. Geological and geochemical background

### 2.1. The Neoarchean Temagami Banded Iron-Formation

The Temagami BIF occurs in the Temagami greenstone belt (a southern appendix to the Abitibi greenstone belt) in Ontario, Canada, which hosts one metasedimentary and four metavolcanic units (Fig. 1). The BIF occurs at the top of the uppermost metavolcanic unit and is associated with turbiditic shales and greywackes, which argues against its deposition at shallow waterdepth. The

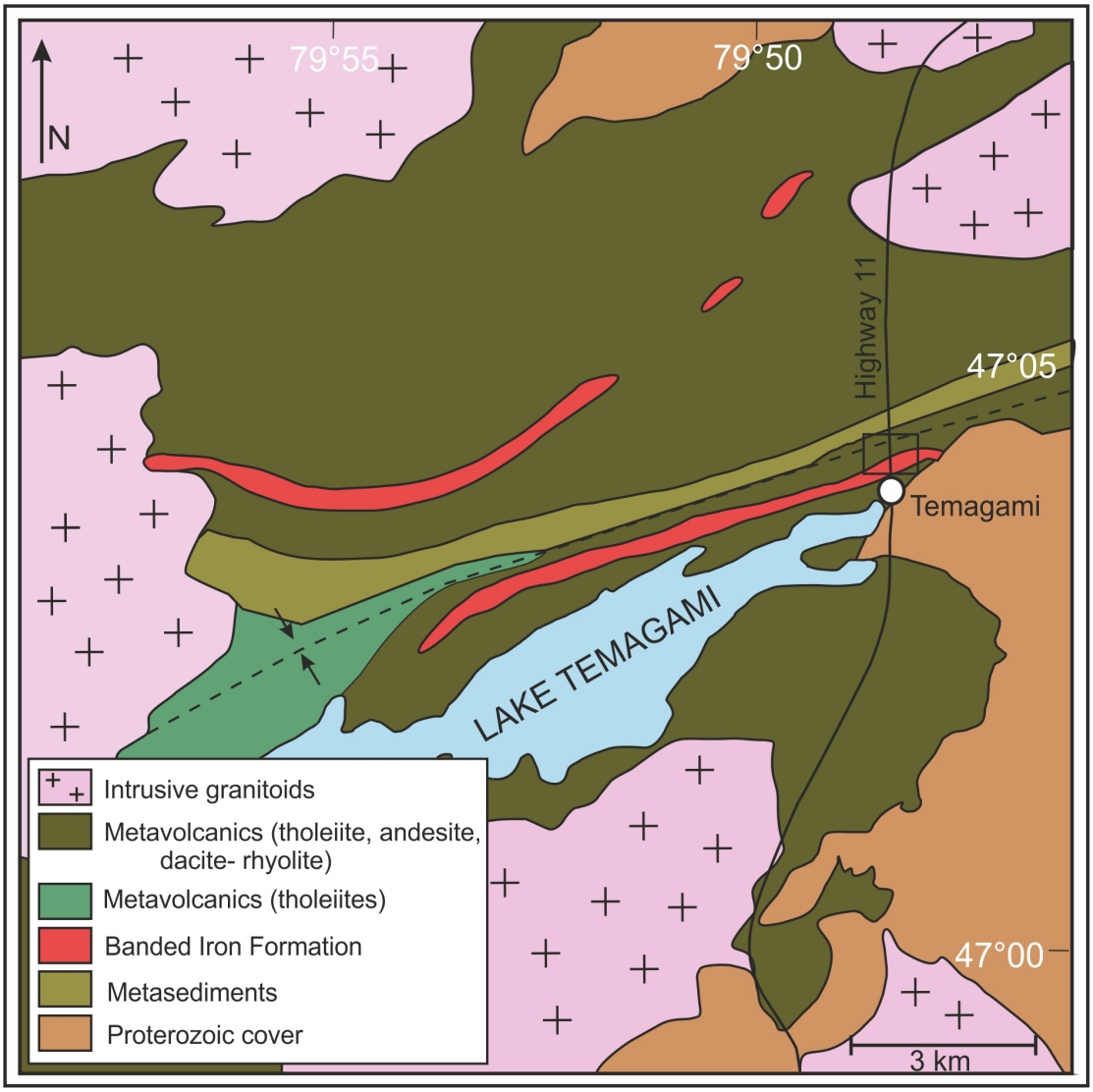


Fig. 1. Simplified geological map of the Lake Temagami area, Ontario, Canada.

succession has been metamorphosed at lower greenschist facies conditions (Bennett, 1978; Fyon and Cole, 1989). In a roadcut built during construction work in the 1990s along Highway 11 just north of the town of Temagami, the chemical sediments constitute an oxide-facies Algoma-type BIF comprised of intercalated magnetite bands with minor hematite, and metachert bands composed of quartz with minor iron-oxide. In contrast to other locations such as the abandonned

Sherman Mine with its prominent bright red jasper beds in the northern limb of the Temagami Greenstone Belt, the samples from the roadcut in the southern part discussed here do not show any sulphide minerals and red jasper is very rare. A Neoarchean depositional age of the Temagami BIF is suggested by U-Pb zircon ages of 2736 ± 3 Ma and 2687 ± 2 Ma for underlying metavolcanics and for a crosscutting rhyolite dike in the overlying andesites, respectively (Bowins and Heaman, 1991). Direct Hf and Nd radiometric dating using individual iron- and silica-rich layers of the Temagami BIF yield an age of 2760 ±120 Ma and 2605 ±140 Ma, respectively (Viehmann et al., 2014), while magnetite samples define a regression line corresponding to an Os age of 2661 ±126 Ma (Schulz et al., 2021). Based on the available data, the age of the Temagami BIF is, therefore, conservatively approximated at 2.7 Ga (e.g., Bowins and Heaman, 1991; Ayer et al., 2006).

Previous work (Bau and Alexander, 2009; Viehmann et al., 2014; Diekrup et al., 2018; Schulz et al., 2021) has shown that the Temagami BIF is a robust high-quality geo-archive of exceptional purity. Its shale-normalized (subscript SN) $REY_{SN}$ patterns (shale is Post-Archean Australian Shale of McLennan, 1989) show the distribution typical of Neoarchean BIFs (and contemporaneous seawater), with light $REY_{SN}$ depletion relative to the heavy $REY_{SN}$, positive anomalies of $La_{SN}$, $Gd_{SN}$ and $Y_{SN}$, and lack of any $Ce_{SN}$ anomaly; some samples even show the W-type lanthanide tetrad effect (Ernst and Bau, 2021). Moreover, the Temagami BIF shows positive $Eu_{SN}$ anomalies and yields positive $\varepsilon Nd_{2.7Ga}$ values, indicating the presence of a high-temperature hydrothermal, probably

mantle-derived component in Temagami seawater (Bau and Alexander, 2009; Viehmann et al., 2014) which is supported by Os isotope data (Schulz et al., 2021). Unusually radiogenic $\varepsilon Hf_{2.7Ga}$ values and decoupled Hf and Nd isotopes in these ultrapure samples further indicate that the Hf was sourced via incongruent terrestrial weathering from intermediate and felsic rocks (Viehmann et al, 2014). This suggests the existence of emerged continental crust ~2.7 Ga ago, that supported a riverine flux of Hf and other elements from this landmass into Temagami seawater. Hence, REY distribution and Nd, Hf and Os isotopes in the Temagami BIF reveal trace element input from two fundamentally different sources (mantle and continental crust) and via two very different pathways (submarine high-temperature hydrothermal fluids and low-temperature continental runoff).

2.2. Geochemical source and redox proxies: Ge-Si-Fe, Cr isotopes and Th-U

From river water and seawater studies (Mortlock and Froehlich, 1987; 1996; Froelich et al., 1989; 1992) it appears that continental runoff shows Ge/Si mass ratios in the range of 0.8 - 3.1 x $10^{-6}$ and that the Ge/Si mass ratio of modern seawater (1.9 x $10^{-6}$) falls right into this range. In contrast, studies of marine high- and low-temperature hydrothermal fluids (Mortlock et al., 1993; Wheat and McManus, 2005; 2008; Escoube et al., 2015) found substantially higher Ge/Si mass ratios of up to 167 x $10^{-6}$. Since the Ge/Si ratio of continental runoff is up to two orders of magnitude lower than that of marine high-temperature hydrothermal fluids, the Ge/Si ratio of marine chemical sediments is considered a

geochemical *source proxy* that reveals the origin of Ge and Si in ambient seawater. The systematic variation of the Ge/Si ratio with the iron concentration or the Fe/Si ratio of Archean BIFs has, therefore, been interpreted (e.g., Hamade et al., 2003; Frei and Polat, 2007; Delvigne et al., 2012; Wang et al, 2014; 2017) to result from the binary mixing of two endmembers: a continent-derived riverine flux best preserved in the (meta)cherts, and a mantle-derived hydrothermal flux best preserved in the iron-(oxyhydr)oxides. This approach, however, has been challenged (Alibert and Kinsley, 2016), as it is argued that the enigmatic banding of BIFs was secondary and developed by separation from an initially homogenous Fe-Si precipitate (e.g., Krapez et al., 2003). The Ge/Si ratios of BIFs, therefore, are by some considered to reflect secondary redistribution, implying major Ge mobility, Ge-Si-Fe fractionation and eventually preferential association of Ge relative to Si with iron (oxyhydr)oxides.

Chromium isotope ratios had initially been assumed to be a rather straightforward *redox proxy* (e.g., Frei et al., 2009; Crowe et al., 2013; Rodler et al., 2015), because the net effect of $Cr^{3+}$ oxidation and $Cr^{6+}$ reduction in oxic surface environments eventually produces seawater that is preferentially enriched in $^{53}Cr$ relative to $^{52}Cr$, with $\delta\ ^{53}Cr$ values above the Bulk Silicate Earth (BSE) array of -0.124 ± 0.101 (Schoenberg et al., 2008). Hence, Cr isotope ratios in marine chemical sediments were supposed to reveal whether this Cr had previously been redox-cycled, and, therefore, may indicate the presence of significant oxygen levels in the source region of this Cr or along its migration path. Positively fractionated $\delta\ ^{53}Cr$ values are observed in a few Archean marine

chemical sediments (e.g., Frei et al., 2009; Crowe et al., 2013). Similarly to other redox proxies such as fractionated Mo and Se isotopes (e.g., Anbar et al., 2007; Duan et al., 2010; Stüeken et al., 2015; Planavsky et al., 2014) and Th/U ratios (e.g., Bau and Alexander, 2009; Partin et al., 2013), fractionated $\delta^{53}Cr$ values in Archean chemical and clastic sediments were interpreted to indicate the existence of temporarily oxygenated surface environments. This, in turn, may suggest the presence photosynthetically produced oxygen already in the Archean, i.e. reflect the existence of transient oxygenated habitats hundreds of millions of years before the GOE that occurred at about 2.4 Ga ago (Luo et al., 2016). However, the $\delta^{53}Cr$ redox proxy, like other geochemical proxies, is controversially discussed and several studies have, indeed, shown or suggested that fractionated $\delta^{53}Cr$ values may result from a range of different processes and may occur in very different geological settings (e.g., Babechuk et al., 2018; Bauer et al., 2019, 2021; Kraemer et al., 2019; and references therein).

The Th/U ratio may also be used as a *redox* proxy. While Th is exclusively tetravalent in natural environments and rather immobile during water-rock interaction, U may be tetravalent or hexavalent, depending on the redox level of the system. In today's oxic atmosphere-hydrosphere system, $U^{4+}$ can be oxidized to U(VI) compounds during weathering. Due to the much higher solubility of U(VI) compared to U(IV) compounds, this results in enhanced mobility of U relative to Th in oxygenated environments, leading to Th-U fractionation and eventually considerably lower Th/U ratios of continental runnoff and seawater compared to the upper crustal Th/U ratio of 3.9. (Rudnick and Gao, 2003). Hence, negatively

206 fractionated Th/U ratios (relative to upper continental crust) in marine chemical
207 sediments reflect low Th/U ratios of ambient seawater and reveal oxidative
208 solubilization of U in Earth's surface environment (Collerson and Kamber, 1999;
209 Bau & Alexander, 2009; Partin et al., 2013).
210
211 **3. Sampling and analytical methods**
212 The micro-drill cores and rock slabs studied originate from BIF specimens
213 sampled in 1999 from a road cut that had been built during construction work at
214 Highway 11 north of the town of Temagami, Ontario, Canada, in the mid-1990s,
215 i.e. only a few years earlier. Where sampled, the outcrop was neither visibly
216 weathered nor covered by lichen, mosses or any other vegetation. Nevertheless,
217 the specimens chosen for this study were split with a rock saw and only the
218 interior of each specimen was used for further study.
219 Concentrations of Ge, Si and Fe have been determined by Laser Ablation
220 - Inductively Coupled Plasma - MassSpectrometry (LA-ICP-MS) on individual
221 sample spots of a 160 µm diameter. The rather large spot size was chosen to
222 avoid the impact of a potential micro-scale redistribution of analytes during
223 neoformation of diagenetic and metamorphic minerals or element clusters, as
224 may be observed in the Hamersley BIFs, Australia (Alibert and Kinsley, 2016).
225 The concentration and isotopic composition of Cr has been determined by
226 Thermal Ionization MassSpectrometry (TIMS) for microdrill cores of 2 mm
227 diameter and ca 10 mm length from individual BIF bands. Chromium isotope
228 ratios are reported as

229 $$\delta\ ^{53}Cr = ((^{53}Cr/^{52}Cr)_{sample}/(^{53}Cr/^{52}Cr)_{SRM979} - 1) \times 1000$$

230 where SRM979 denotes Standard Reference Material 979.

231 The above new results are combined with published data on Th, U, REY and
232 other elements and on Nd and Hf isotopes for individual metachert and magnetite
233 bands from the same hand specimens (data from Bau and Alexander, 2009;
234 Viehmann et al., 2014).

235 More detailed information on the analytical methods employed can be
236 found in the online supplementary material.

237

238 **4. Results**

239 All geochemical data are given in Tables 2 and 3 of the online supplementary
240 material. In all three BIF specimens (TM-1, -2, -3), the concentrations of Fe and
241 Si cover a similarly wide range and as the Fe/Si mass ratio (0.0002 - 82.9),
242 reflect the alternation of metachert and magnetite layers. Germanium
243 concentrations (1.68 - 15.15 mg $kg^{-1}$) correlate with those of Fe ($R^2$ = 0.7754;
244 n=174), but the linear regression (Fig. 2a) indicates that not all Ge is associated
245 with Fe oxides. The Ge/Si mass ratios are between 3.5 x $10^{-6}$ and 390 x $10^{-6}$ and
246 cover a similar range in all three specimens (Fig. 2b and 4a).

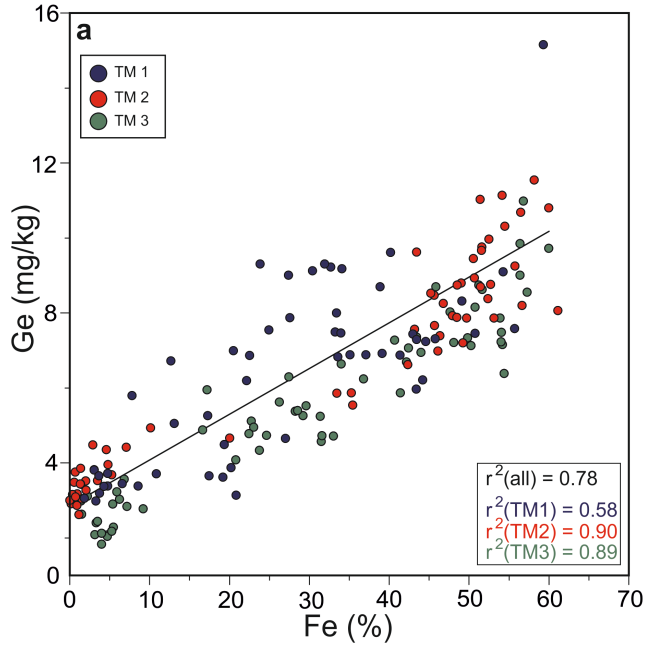


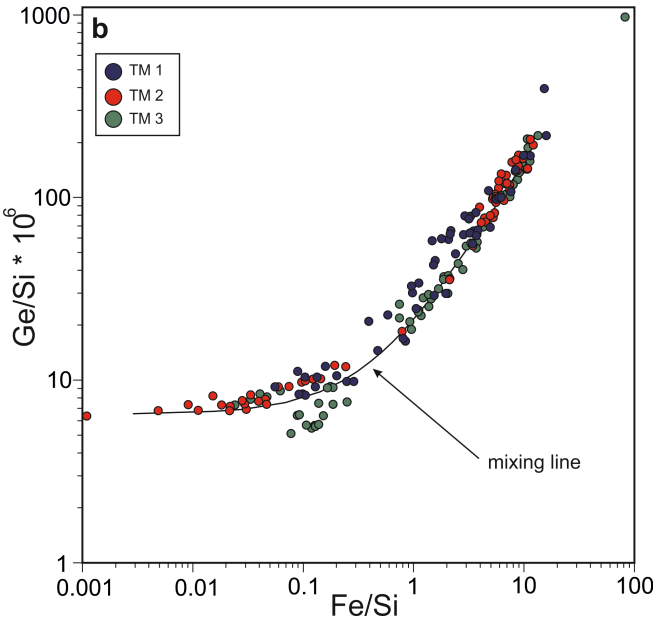


Fig. 2. Graphs of (a) Ge vs Fe concentration and (b) Ge/Si ratio vs Fe/Si ratio. Note that the linear regression line in (a) does not go through the origin, suggesting that not all Ge is associated with iron-oxides, and that in (b) the vast majority of the data fall on a conservative two-component mixing line. For further explanation see text.

In each of the three BIF specimens investigated, Cr concentrations (Fig. 3a) of magnetite bands (1.64 - 6.34 mg $kg^{-1}$) are higher than those of metachert bands

(0.15 - 1.07 mg $kg^{-1}$; and TM-2-2 is exceptional with 2.78 mg $kg^{-1}$ Cr). The $\delta^{53}$Cr values determined for the magnetite bands are negative and fall within a narrow range between -0.16 and -0.01 (Fig. 3b and 4b), i.e. they fall *within* the BSE array of Schoenberg et al. (2008); the only exception is magnetite band TM-1-4 which shows unusually high $\delta^{53}$Cr values between +0.18 and +0.21. In marked contrast, metachert bands show markedly higher $\delta^{53}$Cr values from +0.01 to +0.27 (band TM-2-2 is exceptional again: -0.06), i.e. they show positively fractionated Cr isotope ratios *well-above* the BSE array (Fig. 3b and 4b).

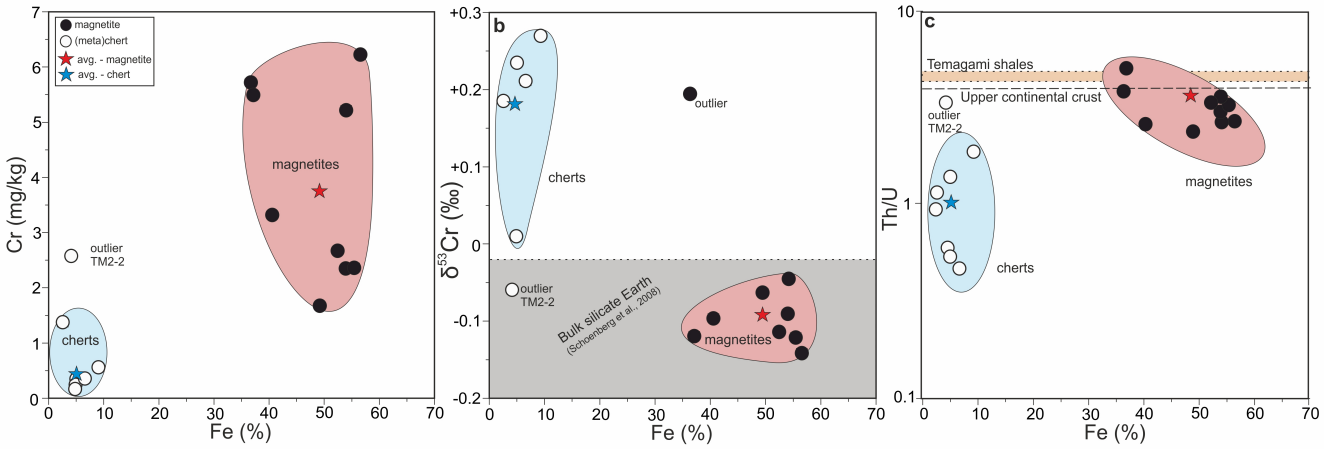


Fig. 3. Graphs of Fe concentration vs (a) Cr concentration, (b) $\delta^{53}$Cr values, and (c) Th/U ratio in iron-rich and silica-rich bands of the Temagami BIF. Note the clear distinction between the geochemical signature of the metachert and the magnetite bands. For further explanation and references see text.

All three BIF specimens show similar ranges of Th/U ratios within magnetite and metachert bands, respectively, but Th/U ratios differ significantly between these two types of bands (Fig. 3c, 4c; see also discussion in Bau and Alexander, 2009). The magnetite bands yield Th/U ratios (2.17 - 5.40) that are close to the upper continental crustal (UCC) ratio of 3.9 (Rudnick and Gao, 2003)

and to the ratios shown by local Temagami shales (4.51 - 4.67), representing the average composition of the exposed landmasses in the Temagami area. In contrast, Th/U ratios in the metachert bands are significantly lower (0.47 - 1.87; one exceptional sample shows Th/U = 3.36), i.e. they are fractionated and significantly lower than the crustal Th/U ratio of UCC and Temagami shales.

Hence, negatively fractionated Th/U ratios coincide with positively fractionated Cr isotopes, but both are confined to the metachert layers with low Ge/Si ratio. In contrast, magnetite layers show unfractionated δ $^{53}$Cr values relative to BSE, unfractionated Th/U ratios similar to UCC and high Ge/Si ratios.

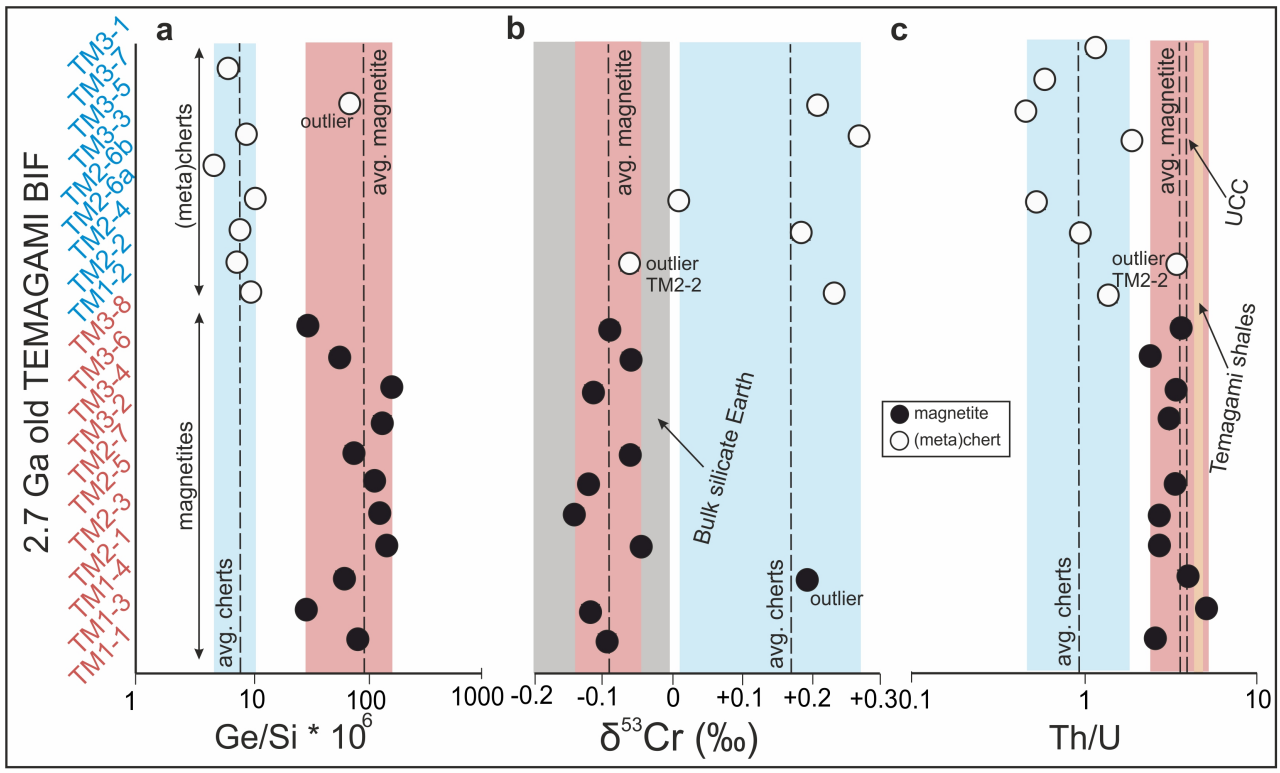


Fig. 4. Graph of (a) Ge/Si, (b) δ $^{53}$Cr values, (c) Th/U ratios of magnetite and metachert bands of the Temagami BIF. UCC: Upper Continental Crust of Rudnick and Gao (2003).

290 **5. Discussion**

291 5.1. Ge-Si-Fe systematics in the Temagami BIF as a source proxy

292 The Ge-Si-Fe characteristics of the Temagami BIF are in full agreement
293 with published data for other BIFs (Hamade et al., 2003; Delvigne et al., 2012;
294 Wang et al., 2014; 2015; Alibert and Kinsley, 2016). In general, Ge/Si and Fe/Si
295 ratios are closely related and follow a conservative two-component mixing line
296 (Fig. 2b) between a silica-rich endmember with a low Ge/Si ratio similar to that of
297 modern continental runoff (0.8-3.1 x $10^{-6}$, Mortlock and Froehlich, 1987) and
298 modern seawater (1.9 x $10^{-6}$, Mortlock and Froehlich, 1996), and an iron-rich
299 endmember with a high Ge/Si ratio that is more similar to what is observed in
300 modern marine hydrothermal fluids (up to 167 x $10^{-6}$; Wheat and McManus,
301 2008). Following the "traditional" interpretation, this suggests that metachert and
302 magnetite bands captured fluid signatures from two distinct sources. Such an
303 interpretation assumes that the Ge-Si couple is not fractionated during the
304 formation of the magnetite and the (meta)chert bands of BIFs, similar to what is
305 observed for the REY. Hence, the magnetite bands in the Temagami BIF with
306 their high Ge/Si ratios that are similar to those of marine hydrothermal fluids,
307 represent episodes of strong hydrothermal Ge and Si input into the ocean,
308 whereas the metachert bands with their low Ge/Si ratios similar to those of
309 modern seawater, recorded episodes when the Ge and Si inventory of seawater
310 was largely derived from continental runoff.

311 An alternative interpretation of Ge-Si-Fe in BIFs (Alibert and Kinsley,
312 2016) assumes that the precursor of the marine chemical sediment was a

313 homogeneous Fe-Si-Ge precipitate and that preferential association of Ge
314 relative to Si with the iron-(oxyhydr)oxides occurred during diagenetic separation
315 of iron-oxide-dominated and silicate-dominated bands, ultimately resulting in
316 higher Ge/Si ratios of the former as compared to the latter. Experimental work by
317 Prokovsky et al. (2006) has indeed shown that Ge is preferentially scavenged
318 relative to Si by iron-(oxyhydr)oxides. The much higher Ge concentrations in the
319 magnetite bands, however, rather suggest that if any diagenetic reset of the
320 Ge/Si ratios occurred, the Ge-poor chert bands should have been more strongly
321 affected than the Ge-rich iron-(oxyhydr)oxide bands. Moreover, it is very unlikely
322 that this diagenetic mobilisation and fractionation affected exclusively the
323 elements Ge and Si. The distribution of the REY, for example, does not support
324 the hypothesis of a secondary origin of the banding. Adjacent iron-oxide and
325 (meta)chert bands in BIFs show very similar Y/Ho ratios (e.g., Ernst and Bau,
326 2021), often combined with different Eu/Sm ratios (e.g., Bau and Dulski, 1992;
327 1996). Similar to Ge, REY concentrations are much higher in the iron-oxide than
328 in the (meta)chert bands. Diagenetic remobilization of REY and subsequent
329 preferential association with iron-(oxyhydr)oxides would produce lower Y/Ho
330 ratios in the iron-oxide bands (see, for example, Bau et al., 2014, for detailed
331 discussion and references) compared to adjacent metachert bands, but very
332 similar Eu/Sm ratios (as fractionation of Eu from Sm requires $Eu^{3+}$ reduction at
333 temperatures (well-)above 200°C; e.g., Bau, 1991; Bau et al., 2010). However,
334 the combination of Ge/Si ratios that are higher, Y/Ho ratios that are lower and
335 Eu/Sm ratios that are similar in iron-oxide bands compared to adjacent

(meta)chert bands is *not* observed in the Temagami or other any BIF, suggesting that the banding of BIFs is, indeed, primary and not a signature of diagenetic processes. The Ge-Si-Fe distribution in the Temagami BIF (Fig. 2, 4a, 5), therefore, strongly suggests that the metachert bands preserved signals from the riverine imprint on Archean seawater. Thus, these metachert bands can be used as indirect archives of conditions and processes on the Archean landmasses. This allows via high-resolution geochemical analysis of pure metachert BIF bands to track the composition of the riverine component in the marine chemical BIF sediment. In contrast, the magnetite bands rather provide geochemical information on the hydrothermal mantle component that episodically affected Temagami seawater during deposition of iron-rich bands.

5.2. Cr isotopes in the Temagami BIF as a redox proxy

When the high-resolution Cr isotope results are combined with the Ge-Si-Fe relationships discussed above (Fig. 4), these data indicate that during times when seawater composition was dominated by continental runoff, its Cr inventory was characterised by positively fractionated $\delta^{53}$Cr isotope values. In contrast, isotopically unfractionated Cr was incorporated into iron-(oxyhydr)oxides during times when seawater carried a strong hydrothermal component from fluids that

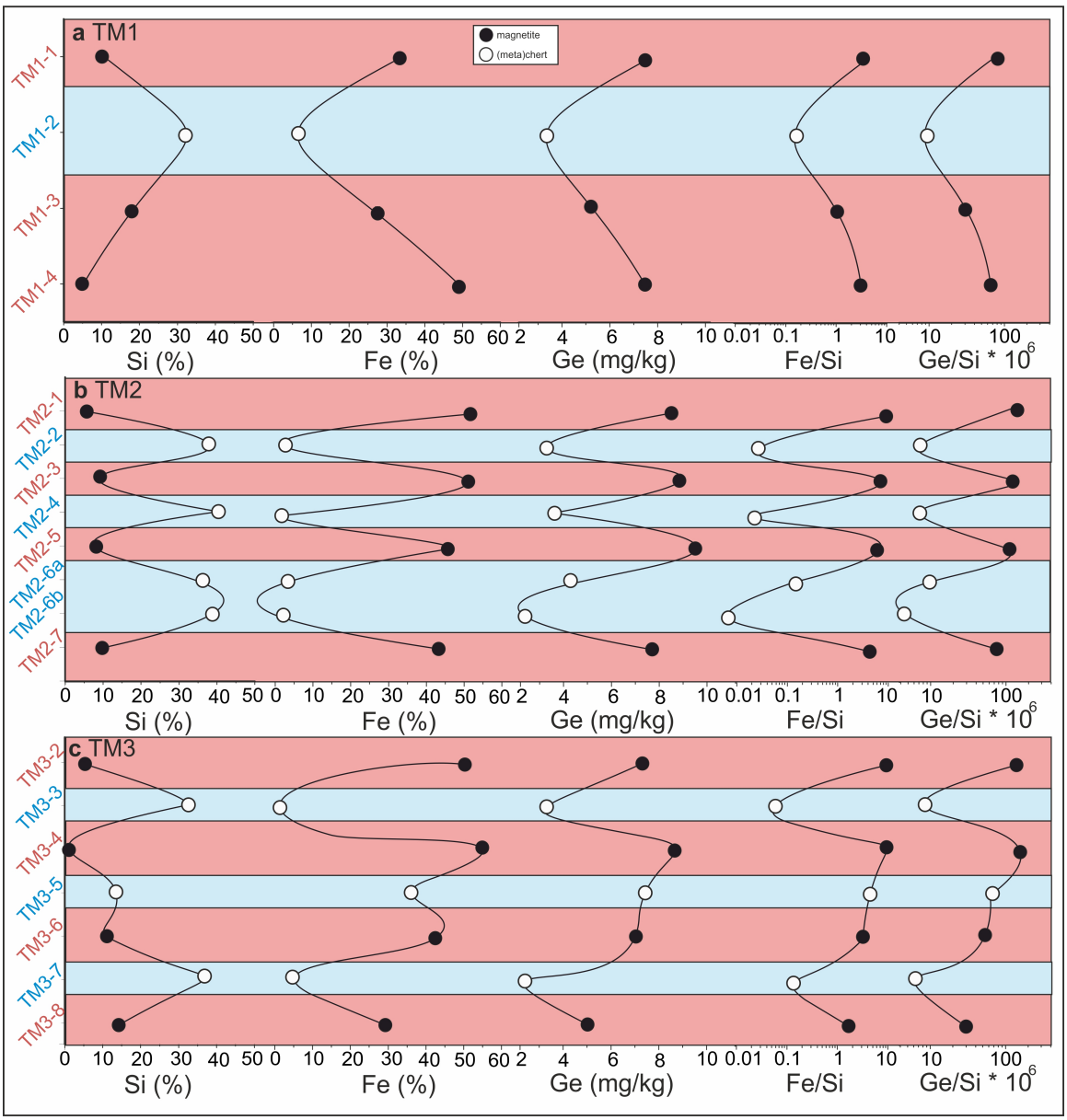


Fig. 5. Systematic variation of Si, Fe, Ge, Fe/Si and Ge/Si between adjacent metachert and magnetite bands in three specimens from the Temagami BIF, Ontario, Canada.

had leached seafloor basalts. Such fluids are reducing and hence transport Cr as Cr(III) species without major isotope fractionation into deep marine ocean water masses. When the dissolved $Fe^{2+}$ which had accumulated in these anoxic, deep marine water masses, was eventually oxidised and formed a layer of iron(III)-oxyhydroxides, these precipitates scavenged the hydrothermal Cr. Since this

mantle Cr had never been oxidized throughout the mobilisation-immobilisation sequence in anoxic, deep marine Temagami seawater, it remained unfractionated and shows δ $^{53}$Cr values similar to BSE (e.g., Bauer et al., 2019). In contrast, during times of iron-poor chert deposition, the riverine flux which transported Ge and Si (and very radiogenic Hf; Viehmann et al., 2014), carried isotopically fractionated Cr into the ocean, similar to modern rivers (e.g., D'Arcy et al., 2016; Wu et al., 2017). As Cr isotope fractionation occurs in the presence of free oxygen that allows to mobilise Cr as Cr(VI), these data may be indirect evidence of oxidative weathering of emerged continental crust and oxygenic photosynthesis at ~2.7 Ga ago.

Although organic-ligand-promoted mobilization of Cr may also produce positively fractionated Cr isotope ratios (e.g., Saad et al., 2017; Kraemer et al., 2019), it seems unlikely that such ligands had been abundant enough in Neoarchean freshwater systems to control the Cr isotopic composition of continental runoff in an oxygen-free to -poor environment (e.g., Saad et al., 2017). The data presented here, therefore, rather suggest that during deposition of the Temagami BIF 2.7 billion years ago, Cr isotope fractionation occurred in and was confined to a terrigenous environment which allowed for the redox cycling of Cr.

The association of unfractionated δ $^{53}$Cr values and high Ge/Si ratios with iron-oxide bands and of positively fractionated δ $^{53}$Cr values and low Ge/Si ratios with metachert bands (Fig. 5, 6) is additional evidence from two very different geochemical proxies that these alternating layers of two types of marine

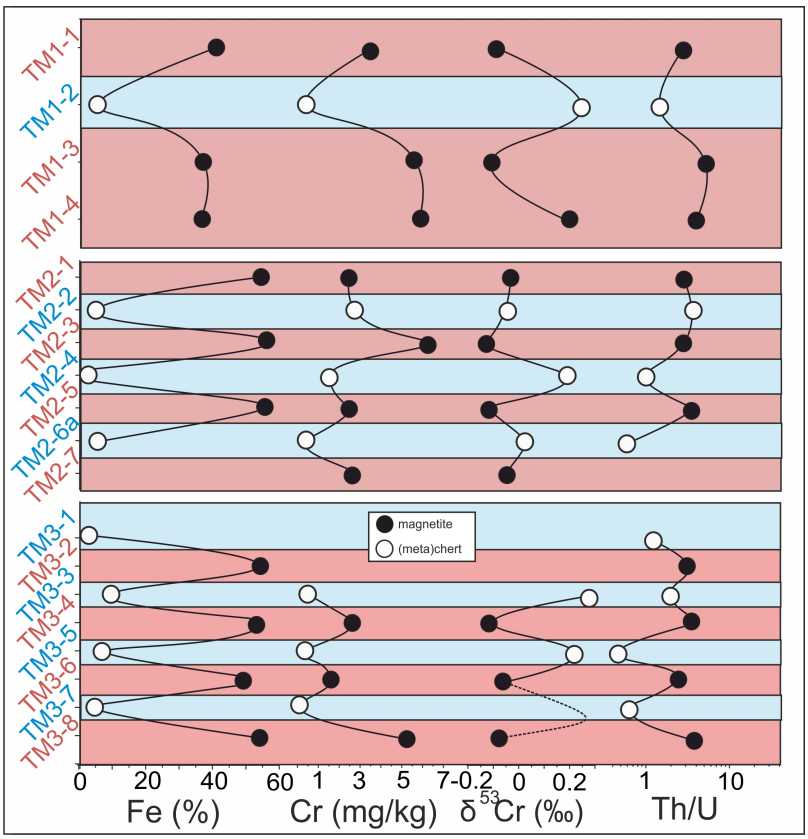


Fig. 6. Systematic variation of Fe, Cr, δ $^{53}$Cr and Th/U between adjacent metachert and magnetite bands in three specimens from the Temagami BIF, Ontario, Canada.

precipitates formed from different water masses. This corroborates that the hitherto enigmatic banding of BIFs is a primary depositional feature and was not produced during or even after diagenesis from an initially homogeneous Fe-Si precursor.

5.3. Th-U relationships in the Temagami BIF as a redox proxy

Since the use of Cr isotopes as redox proxy is complex and hence controversially discussed, Th-U relationships as an additional redox proxy may help to put a Cr-based interpretation into perspective. In marked contrast to the magnetite bands, the metachert bands not only show fractionated Cr isotope

401 ratios but also negatively fractionated Th/U ratios (Fig. 3c, 4c), suggesting
402 preferential riverine input of U relative to Th into seawater. Such fractionation of
403 the Th-U couple, however, requires oxidation of $U^{4+}$ and stabilisation of water-
404 soluble U(VI) compounds (e.g., Collerson and Kamber, 1999; Partin et al., 2013).
405 Although organic complexation of U and Th with ligands such as siderophores
406 may preferentially mobilize U relative to Th (Bau et al., 2013, Kraemer et al.,
407 2015) as is observed for Cr and its isotopes (Saad et al., 2017; Kraemer et al.,
408 2019), this is unlikely to have happened in the Neoarchean at a scale large
409 enough to control Th-U behaviour in continental runoff. Moreover, it is not yet
410 known whether this siderophore-promoted Th-U fractionation can also occur in
411 an oxygen-free environment.
412 Hence, the combination of high-resolution Cr isotope, Ge/Si and Th/U data
413 reveals that positively fractionated Cr isotopes and negatively fractionated Th/U
414 ratios are confined to the metachert bands with low Ge/Si ratios, which captured
415 input from terrestrial environments, but that both features evidently are absent
416 from the hydrothermally impacted marine deep waters whose composition was
417 recorded by the magnetite bands that show high Ge/Si ratios (Fig. 6). Besides
418 corroborating the primary nature of BIF bands, this lends further credence to the
419 use of Cr isotopes as a paleo-redox proxy, at least in the Neoarchean Temagami
420 BIF, and suggests a period of active redox-cycling of Cr in the Neoarchean
421 Earth's surface system ca 400 million years before the GOE.
422
423

## 6. Conclusion

High-resolution multi-proxy data for the ca 2.7 Ga old Temagami BIF provide information on element sources to the Archean ocean and on the redox level in these source regions. The alternating deposition of (i) iron-(oxyhydr)oxides (now magnetite) with high Ge/Si ratios, unfractionated Cr isotopes and crustal, i.e. unfractionated Th/U ratios, and (ii) cherts (now metachert) with low Ge/Si ratios, positively fractionated Cr isotopes and negatively fractionated Th/U ratios in the “Temagami Sea” to form a BIF that also shows decoupled Hf and Nd isotopes (Viehmann et al., 2014) suggests that ~2.7 Ga ago, emerged landmasses were temporarily altered by oxidative weathering and that this oxygenated terrestrial environment coexisted with an anoxic ocean. The composition of local seawater in the Temagami Sea was periodically controlled by either hydrothermally dominated ferrous iron-rich marine deep water masses or by continental runoff from this oxygenated terrestrial environment. This generated two different marine water masses, each with a distinctive geochemical signature, from which the alternating chert and iron-(oxyhydr)oxide chemical sediments precipitated, which produce the prominent banding of BIFs. The combined evidence from several geochemical proxies argues for a primary origin of the banding of BIFs rather than for a diagenetic separation of iron- and silica-bands from an initially geochemically homogenous precipitate. The ultrapure oxide-facies Temagami BIF sampled at the roadcut at Highway 11 in Ontario, Canada, appears to be a unique archive of Neoarchean seawater, and complementary studies with a focus on other geochemical proxies should be able to provide a wealth of

447 additional information on the Neoarchean atmosphere-hydrosphere system.

448

449 **REFERENCES**

450

451 Alexander, B. W., Bau, M., Andersson, P., 2009- Neodymium isotopes in
452 Archean seawater and implications for the marine Nd cycle in Earths early
453 oceans. Earth Planet. Sci. Lett. 283, 144-155.

454

455 Alibert, C., Kinsley, L., 2016. Ge/Si in Hamersley BIF as tracer of hydrothermal Si
456 and Ge inputs to the Paleoproterozoic ocean. Geochim. Cosmochim. Acta 184,
457 329-343.

458

459 Anbar, A.D., Duan, Y., Lyons, T.W., Arnold, G.L., Kendall, B., Creaser, R.A.,
460 Kaufman, A.J., Gordon, G.W., Scott, C., Garvin, J., Buick,R., 2007, A whiff of
461 oxygen before the Great Oxidation Event? Science 317, 1903-1906.

462

463 Ayer, J.A., Chartrand, J.E., Grabowski, G.D.P., Josey, S., Rainsford, D., Trowell,
464 N.F., 2006. Geological compilation of the Cobalt–Temagami area, Abitibi
465 greenstone belt. Ontario Geological Survey, Preliminary Map, 3581.

466

467 Babechuk, M.G:, Kleinhanns, I.C., Reitter, E., Schoenberg, R., 2018. Kinetic
468 stable Cr isotopic fractionation between aqueous Cr(III)-Cl-$H_2O$ complexes at
469 25 °C: Implications for Cr(III) mobility and isotopic variations in modern and
470 ancient natural systems. Geochimica et Cosmochimica Acta 222, 383-405.

471

472 Bau, M., 1991. Rare earth element mobility during hydrothermal and
473 metamorphic fluid-rock interaction and the significance of the oxidation state of
474 europium. Chem. Geol. 93, 219-230.

475

476 Bau, M., Alexander, B. W., 2009. Distribution of high field strength elements (Y,

Zr, REE, Hf, Ta, Th, U) in adjacent magnetite and chert bands and in reference standards FeR-3 and FeR-4 from the Temagami iron-formation, Canada, and the redox level of the Neoarchean ocean. Precam. Res. 174, 337-346.

Bau, M., Dulski, P., 1992. Small-scale variations of the rare-earth element distribution in Precambrian iron-formations. Eur. J. Min. 4, 1429-1433.

Bau, M., Dulski, P., 1996. Distribution of yttrium and rare-earth elements in the Penge and Kuruman Iron-Formations, Transvaal Supergroup, South Africa. Precambrian Res. 79, 37-55.

Bau, M., Balan, S., Schmidt, K., Koschinsky, A., 2010. Rare earth elements in mussel shells of the Mytilidae family as tracers for hidden and fossil high-temperature hydrothermal systems. Earth and Planet. Sci. Lett. 299, 310–316.

Bau, M., Tepe, N., Mohwinkel, D., 2013. Siderophore-promoted transfer of rare earth elements and iron from volcanic ash into glacial meltwater, river and ocean water. Earth Planet. Sci. Lett. 364, 30–36.

Bau, M., Schmidt, K., Koschinsky, A., Hein, J., Kuhn, T., Usui, A.,2014. Discriminating between different genetic types of marine ferro-manganese crusts and nodules based on rare earth elements and yttrium. Chemical Geology 381, 1–9.

Bauer, K.W., Cole, D.B., Asael, D., Francois, R., Calvert, S.E., Poulton, S.W., Planavsky, N.J., Crowe, S.A., 2019. Chromium isotopes in marine hydrothermal sediments. Chemical Geology 529, 119286.

Bauer, K.W., Planavsky, N.J., Reinhard, C.T., Cole, D.B., 2021. The chromium isotope system as a tracer of ocean and atmosphere redox. Cambridge University Press, 34p.

Bekker, A., Planavsky, N. J., Krapez, B., Rasmussen, B., Hofmann, A., Slack, J. F., Rouxel, O. J., Konhauser, K. O., 2014. Iron formations: their origins and implications for ancient seawater chemistry. In: Holland H, Turekian K (eds) Treatise on geochemistry. Elsevier, Waltham, pp. 561-625.

Collerson, K. D., Kamber, B.S., 1999. Evolution of the continents and the atmosphere inferred from Th-U-Nb systematics of the depleted mantle. Science 283, 1519-1522.

Crowe, S. A., Dossing, L. N., Beukes, N. J., Bau, M., Kruger, S. J., Frei, R., Canfield, D.E., 2013. Atmospheric oxygenation three billion years ago. Nature, 501, 535-539.

D'Arcy, J., Babechuk, M. G., Dossing, L. N., Gaucher, C., Frei, R., 2016. Processes controlling the chromium isotopic composition of river water: constraints from basaltic river catchments. Geochim. Cosmochim. Acta 186, 296–315.

Delvigne C., Cardinal D., Hofmann A., André, L., 2012. Stratigraphic changes of Ge/Si, REE+Y and silicon isotopes as insights into the deposition of a Mesoarchaean banded iron formation. Earth Planet. Sci. Lett., 355/356, 109-118.

Diekrup, D., Hannington, M. D., Strauss, Ginley, S. J., 2018. Decoupling of Neoarchean sulfur sources recorded in Algoma-type banded iron formation. Earth Planet. Sci. Lett. 489, 1-7.

Duan, Y., Anbar, A. D., Arnold, G. L., Lyons, T. W., Gordon, G.W., Kendalla, B., 2010. Molybdenum isotope evidence for mild environmental oxygenation before the Great Oxidation Event. Geochim. Cosmochim. Acta 74, 6655-6668.

Eickmann, B., Hofmann, A., Wille, M., Bui, T. H., Wing, B. A., Schoenberg R., 2018. Isotopic evidence for oxygenated Mesoarchaean shallow oceans. Nature Geosci. 11, 133-138.

Ernst, D.M., Bau, M., 2021. Banded iron formation from Antarctica: The 2.5 Ga old Mt. Ruker BIF and the antiquity of lanthanide tetrad effect and super-chondritic Y/Ho ratio in seawater. Gondwana Research 91, 97-111; DOI: 10.1016/j.gr.2020.11.011

Frei, R., Polat, A., 2007. Source heterogeneity for the major components of <3.7 Ga Banded Iron Formations (Isua Greenstone Belt, Western Greenland): tracing the nature of interacting water masses in BIF formation. Earth Planet. Sci. Lett., 253, 266-281.

Frei, R., Gaucher, C., Poulton, S. W. Canfield, D. E., 2009. Fluctuations in Precambrian atmospheric oxygenation recorded by chromium isotopes. Nature 461, 250-253.

Hamade, T., Konhauser, K. O., Raiswell, R., Goldsmith, S., Morris, R. C., 2003, Using Ge/Si ratios to decouple iron and silica fluxes in Precambrian banded iron formations. Geology 31, 35-38.

Kraemer, D., Kopf, S., Bau, M., 2015. Oxidative mobilization of cerium and uranium and enhanced release of “immobile” high field strength elements from igneous rocks in the presence of the biogenic siderophore desferrioxamine-B. Geochim. Cosmochim. Acta 165, 263-279.

Kraemer D., Frei R., Viehmann S., Bau M., 2019. Mobilization and isotope fractionation of chromium during water-rock interaction in presence of siderophores. Applied Geochemistry 102, 44-54.

570 Krapez, B., Barley, M. E., Pickard, A. L., 2003. Hydrothermal and resedimented
571 origins of the precursor sediments to banded iron formations: Sedimentological
572 evidence from the early Palaeoproterozoic Brockman Supersequence of Western
573 Australia. Sedimentology 50, 979-1011.
574
575 Luo, G., Ono, S., Beukes, N. J., Wang, D. T., Xie, S., Summons, R. E., 2016.
576 Rapid oxygenation of Earth's atmosphere 2.33 billion years ago. Science
577 Advances 2, 5.
578
579 McLennan, S.M., 1989. Rare earth elements in sedimentary rocks: influence of
580 provenance and sedimentary processes. In: Lipin, B.R., McKay, G.A. (Eds.),
581 Geochemistry and Mineralogy of Rare Earth Elements. Mineral. Soc. Am.,
582 Washington, DC, pp. 169–200.
583
584 Mortlock, R. A., Froelich, P. N., 1987. Continental weathering of germaniumGe/Si
585 in the global river discharge. Geochim. Cosmochim. Acta 51, 2075-2082.
586
587 Mortlock, R. A., Froelich, P. N., 1996. Determination of germanium by isotope
588 dilution-hydride generation inductively coupled plasma mass spectrometry. Anal.
589 Chim. Acta 332, 277-284.
590
591 Mortlock R. A., Froelich P. N., Feely R. A., Massoth G. J., Butterfield D. A.,
592 Lupton, J.E., 1993. Silica and germanium in Pacific Ocean hydrothermal vents
593 and plumes. Earth Planet. Sci. Lett. 119, 365–378.
594
595 Partin, C. A., Lalonde, S. V., Planavsky, N. J., Bekker, A., Rouxel, O. J., Lyons,
596 T. W., Konhauser, K. O., 2013. Uranium in iron formations and the rise of
597 atmospheric oxygen. Chem. Geol. 362, 82-90.
598
599 Planavsky, N.J., Asael, D., Hofmann, A., Reinhard, C.T., Lalonde, S.V.,
600 Knudsen, A., Wang, X., Ossa Ossa, F., Pecoits, E., Smith, A.J.B., Beukes, N.J.,

Bekker, A., Johnson, T.M., Konhauser, K.O., Lyons, T.W., Rouxel, O.J., 2014. Evidence for oxygenic photosynthesis half a billion years before the Great Oxidation Event. Nature Geosci. 7, 283-286.

Pokrovsky O. S., Pokrovski G. S., Schott J., Galy A., 2006. Experimental study of germanium adsorption on goethite and germanium coprecipitation with iron hydroxide: X-ray absorption fine structure and macroscopic characterization. Geochimica et Cosmochimica Acta 70, 3325–3341.

Rodler, A., Sanchez-Pastor, N., Fernandez-Diaz, L., Frei, R., 2015. Fractionation behavior of chromium isotopes during coprecipitation with calcium carbonate: implications for their use as paleoclimatic proxy. Geochim. Cosmochim. Acta 164, 221-235.

Rudnick, R. L., Gao, S., 2003. 3.01 - Composition of the Continental Crust. Treatise on Geochemistry 3, 1-64.

Saad, E.M., Wang, X., Planavsky, N.J., Reinhard, C.T., Tang, Y., 2017. Redox-independent chromium isotope fractionation induced by ligand-promoted dissolution. Nature Communications 8, 1590.

Schoenberg, R., Zink, S., Staubwasser, M., von Blanckenburg, F., 2008. The stable Cr isotope inventory of solid Earth reservoirs determined by double spike MC-ICP-MS. Chem. Geol. 249, 294-306.

Schulz, T., Viehmann, S., Hezel, D.C., Koeberl, C., Bau, M., 2021. Highly siderophile elements and coupled Fe-Os isotope signatures in the Temagami Iron Formation, Canada: Possible signatures of Neoarchean seawater chemistry and Earth's oxygenation history. Astrobiology 21/8, DOI: 10.1089/ast.2020.2311

Stüeken, E. E., Buick, R. & Anbar, A. D., 2015. Selenium isotopes support free

$O_2$ in the latest Archean. Geology 43, 259-262.

Viehmann, S., Hoffmann, J. E., Münker, C., Bau, M., 2014. Decoupled Hf-Nd isotopes in Neoarchean seawater reveal weathering of emerged continents. Geology 42, 115-118.

Viehmann, S., Bau, M., Hoffmann, J. E., Münker, C., 2015. Geochemistry of the Krivoy Rog Banded Iron Formation, Ukraine, and the impact of peak episodes of increased global magmatic activity on the trace element composition of Precambrian seawater. Precam. Res. 270, 165-180.

Wang, C., Zhang, L., Dia, Y., Li, W., 2014. Source characteristics of the ~2.5 Ga Wangjiazhuang Banded Iron Formation from the Wutai greenstone belt in the North China Craton: Evidence from neodymium isotopes. J. Asian Earth Sci. 93, 288-300.

Wang, C., Wu, H., Li, W., Peng, Z., Zhang, L., Zhai, M., 2017. Changes of Ge/Si, REE+Y and Sm-Nd isotopes in alternating Fe- and Si-rich mesobands reveal source heterogeneity of the ~2.54 Ga Sijiaying banded iron formation in Eastern Hebei, China. Ore Geol. Rev. 80, 363-376.

Wheat C. G., McManus J., 2005. The potential role of ridge- flank hydrothermal systems on oceanic germanium and silicon balances. Geochim. Cosmochim. Acta 69, 2021–2029.

Wheat, C. G., McManus, J., 2008. Germanium in mid-ocean ridge flank hydrothermal fluids. Geochem. Geophys. Geosyst. 9.

Wu, W.H., Wang, X.L., Reinhard, C.T., Planaysky, N.J., 2017. Chromium isotope systematics in the Connecticut River. Chemical Geology, 456: 98-111.

**Acknowledgements** M.B. acknowledges the help of Brian Alexander (now Inorganic Ventures Inc.) during sampling in Ontario and cooperation and discussion with participants of and funding through DFG Priority Program 1833 “Building a Habitable Earth” (grant BA-2289/8-1). R.F. acknowledges funding through the Danish Agency for Science, Technology and Innovation (grant 11-103378) and thanks Toby Leeper for maintaining the mass spectrometers in perfect running condition and Toni Larsen for lab-assistance. D.G. acknowledges the help of Ulrike Westernströer (Kiel University) with LA-ICP-MS analyses. S.V. acknowledges funding from the European Unions Horizon 2020 research and innovation program of the Marie Sklodowska-Curie grant agreement No 746033 for project ELEMIN.

**Author Contributions** M.B. initiated, coordinated and provided the samples for this study and wrote the manuscript with contributions from all co-authors; R.F. did Cr isotope measurements and TIMS data processing; D.G. did Ge-Si-Fe measurements and LA-ICP-MS data processing; S.V. did all other geochemical analyses and all artwork.

# SUPPLEMENTARY MATERIAL

## 1. Analytical Methods

### *1.1. Determination of concentrations of Ge, Si and Fe by Laser Ablation - Inductively Coupled Plasma - Mass Spectrometry (LA-ICP-MS)*

*In-situ* microanalyses of Ge, Si and Fe concentrations of individual metachert and Fe-oxide layers in polished slabs of Temagami BIF samples TM-1, TM-2, and TM-3 have been accomplished by laser ablation – inductively coupled plasma - mass spectrometry (LA-ICP-MS) using a homogenized 193nm ArF excimer laser (GeoLas HD, Coherent) with a fast-washout two-volume ablation cell (LDHCLAC; Fricker et al., 2011) that was coupled to a fast quadrupole instrument (7900s, Agilent) operated in standard mode. Helium (1.0 L $min^{-1}$) with addition of $H_2$ (0.014 l $min^{-1}$) was used as the carrier gas. Plasma conditions were monitored at U/Th ≈ 1.05 and ThO/Th <0.2 %.

In ICP-MS the elements Si, Fe, and Ge are affected by interferences from polyatomic ions originating mainly from the ICP: $[^{14}N_2]^+$, $[NO]^+$, $[NOH]^+$, $[CO]^+$ and $[COH]^+$ affect Si on 28, 29 and 30 (m/z; mass-to-charge-ratio), and $[ArO]^+$ and $[ArOH]^+$ affect Fe on 56 and 57 (m/z) but can be corrected for by careful monitoring and subtraction of gas background signals. In contrast, all Ge isotopes are interfered by $[FeO]^+$ and $[FeOH]^+$ originating from the BIF sample matrix. Consequently, these interferences need a correction procedure on basis of actual (FeO/Fe) and (FeOH/Fe) formation rates. We used a natural magnetite (UQAC-C28, pers. comm. D. Savard) and determined formation rates (FeO/Fe) of 1.04 ± 0.07 E-5, 0.56 ± 0.12 E-5, and 0.21 ± 0.01 E-5 on 72, 73, and 74 (m/z). For quantification of Si, Fe, and Ge, interference-corrected signals on 29, 57, and 74 (m/z) were used.

Each individual metachert or magnetite band was sampled with two clusters of four laser spots (each spot 160 µm in diameter). This rather large spot size minimized the impact of a potential redistribution of analytes during neoformation of diagenetic and metamorphic minerals or element clusters from the initially amorphous chert or iron-oxyhydroxide precipitates (Alibert and Kinsley, 2016). The reported data represent blank-subtracted averages. Data acquisition was over 40 s after 20 s background measurement with laser off. The definition of integration windows in the time-resolved spectra was done graphically using the GLITTER software package. That integrated data set was transferred to spreadsheet software for subsequent data processing and calibration. The certified BIF reference materials Fer-3, Fer-4, and IF-G were re-processed at University Kiel to nano-particulate pressed powder pellets (Garbe-Schönberg and Müller, 2014) labeled Fer-3-P, Fer-4-P, and IF-G-P, which were then used for matrix-matched calibration utilizing recommended values from the GeoReM online data base (Table S1). Analytical error was estimated from replicate analyses of the nano-powder pellets and found to be better than 0.5-3 % RSD (1SD) for Ge/Si, and <5 % RSD for Si, Fe, and Ge.

**Supplementary Table 1:** Quantitative results for reference materials prepared as nano-particulate pressed powder pellets (-P) compared to recommended values (recomm.).

| Element | Mass fraction | IF-G recomm. | IF-G-P | Fer-3 recomm. | Fer-3-P | Fer-4 recomm. | Fer-4-P |
|---|---|---|---|---|---|---|---|
| Si | mg $g^{-1}$ | 192.6 | 186.6 | 250.6 | 259.6 | 233.7 | 254.3 |
| Fe | mg $g^{-1}$ | 390.3 | 378.6 | 311.2 | 322.2 | 279.8 | 295.3 |
| Ge | mg $g^{-1}$ | 0.024 | 0.0233 | 0.004 | 0.0043 | 0.005 | 0.0064 |
| Ge/Si*10E6 | | 125 | 124 | 16 | 17 | 24 | 25 |

*1.2. Determination of δ $^{53}$Cr by Thermal Ionization Mass Spectrometry (TIMS)*

Individual cored out samples were crushed in an agate shatter mill. Fifty to one hundered mg of sample powders were dissolved in 7 ml Savillex™ beakers in a mixture of 2 ml concentrated HF and 3 ml of aqua regia (all Seastar™ acids) for 48 hours. The samples were doped with an appropriate amount of a $^{50}$Cr-$^{54}$Cr double spike. After 48 hours on a hotplate at 130 °C, the sample solutions were dried down. The samples first were re-dissolved in 6 N HCl and passed over a chromatographic column charged with 12 ml of an anion exchange resin, according to the procedure described in Frei et al. (2009) for the purpose of removing the iron matrix from the samples. After renewed evaporation of the Cr-cuts, the samples were then re-dissolved in 10 ml of 0.1 N HCl to which 3 drops of a 10% ammonium hydroxide solution and 3 drops of concentrated $H_2O_2$ were added to enable oxidation of Cr(III) to Cr(VI). After about 12 hours, the sample solution was then passed over PP extraction columns charged with 2 ml anion resin (Biorad ™ AG-1 × 8, 100–200 mesh). Cr(VI), retained in the resin, was released by reduction to Cr(III) with the help of 10 ml 0.1 $HNO_3$ doped with 3 drops of concentrated $H_2O_2$ into 12 ml Savillex™ Teflon beakers. After drying of this sample on a hotplate at 100 °C, the sample was re-dissolved in 150 µ l of 8N HCl and, with the lid closed, was placed on a hotplate at 100 °C for 15 minutes, during which the beaker was repeatedly tapped to prevent the solution in the beaker evaporating and fully condensing on the beaker's surface. The sample was then diluted with 2.5 ml ultraclean water and passed over 2 ml of cation exchange resin (AG 50W-8, 200–400 mesh) charged PP columns. The extraction procedure followed a slightly modified recipe of Bonnand et al. (2011) and Trinquier et al. (2008). With applying a three ion chromatographic column procedure we obtain highly pure Cr separates. Disturbing cations and anions are efficiently removed from the sample solutions during the oxidation-reduction step in the anion chromatographic separation, whereas remaining cations such as $Ca^{2+}$, $Na^{+}$, and $Mn^{2+}$ are removed in the respective elution procedure over the cation exchange column.

Chromium separates were measured on an IsotopX, model “Phoenix” TIMS, equipped with eight moveable Faraday collectors, in static mode. Loading and measuring procedures adhere to those reported by Frei and Polat (2013). We report Cr isotope compositions as $\delta\ ^{53}Cr = (^{53}Cr/^{52}Cr)_{sample}/(^{53}Cr/^{52}Cr)_{SRM\ 979} - 1) \times 1000$, where SRM 979 denotes Standard Reference Material 979. We presently measure and externally reproduce the double spiked SRM 979 Cr standard at $\delta\ ^{53}Cr$ = 0.05 + /− 0.08‰ (n = 345), with maintaining a $^{52}Cr$ signal at 5E-12 Ampères (corresponding to a 500 mV beam intensity which we usually aim at for our sample analyses). A double spiked SRM 979 standard was irregularly interspersed in our analytical batches, in that way that a standard measurements was performed between every 3 to 4 sample measurements. The reported $\delta\ ^{53}Cr$ values and respective errors of the samples are calculated as the average of “n” repeated mass spectrometrical runs with their two standard deviations and include the correction for the offset of + 0.05% for our SRM 979 from its accepted 0‰ δ 53Cr value. A mass spectrometrical run consisted of 120 scans (divided in 12 blocks) with a signal integration period of ten seconds for each scan. Baselines were measured at the beginning of every second block over an integration period of 20 seconds each at + 0.5 and − 0.5 AMU from the Cr peaks. A typical mass spectrometrical run lasted ~40 minutes. Procedural Cr blanks were in the order of 2–4 ng and are insignificant relative to sample Cr amounts > 350 ng (but typically $\gg$500 ng), i.e., they did not affect the measured Cr isotope composition of the samples.

During the time period where we measured our samples, we have interspersed analyses of the iron formation standard IF-G (Govindaraju, 1984). This standard was prepared from quartz-magnetite BIF of the IGB (Isua Greenstone Belt) and is therefore a suitable material for comparative purposes with our micro-drilled core samples. $\delta\ ^{53}Cr$ values of two independently processed aliquots of the IF-G standard agree with the results of the IF-G standard published in Frei et al. (2016) with an average $\delta\ ^{53}Cr$ value of 0.02 + /− 0.07%.

## 2. Supplementary References


Alibert, C. & Kinsley, L. Ge/Si in Hamersley BIF as tracer of hydrothermal Si and Ge inputs to the Paleoproterozoic ocean. Geochim. Cosmochim. Acta, 184, 329-343 (2016).

Bonnand, P., Parkinson, I. J., James, R. H., Karjalainen, A.-M. & Fehr, M. A. Accurate and precise determination fo stable Cr isotope compositions in carbonates by double spike MC-ICP-MS. J. Anal. At. Spectrom. 26, 528–536 (2011).

Frei, R. & Polat, A. Chromium isotope fractionation during oxidative weathering - Implications from the study of a Paleoproterozoic (ca. 1.9 Ga) paleosol, Schreiber Beach, Ontario, Canada. Precambr. Res. 224, 434–453 (2013).

Frei, R., Gaucher, C., Poulton, S. W. & Canfield, D. E. Fluctuations in Precambrian atmospheric oxygenation recorded by chromium isotopes. Nature 461, 250–253 (2009).

Fricker, M. B., Kutscher, D., Aeschlimann, B., Frommer, J., Dietiker, R., Bettmer, J. & Günther, D. High spatial resolution trace element analysis by LA-ICP-MS using a novel ablation cell for multiple or large samples. Int. J. Mass Spectrom. 307, 39–45 (2011).

Garbe-Schönberg, D. & Müller, S. Nano-particulate pressed powder tablets for LA-ICP-MS. J. Anal. At. Spectrom. 29, 990-1000 (2014).

Govindaraju, K. Compilation of working values and sample description for 383 geostandards. Geostandards Newslett. 18, 1–158 (1994).

Trinquier, A., Birck, J. L. & Allègre, C. J. High-precision analysis of chromium isotopes in terrestrial and meteorite samples by thermal ionization mass spectrometry. J. Anal. At. Spectrom. 23, 1565–1574 (2008).

## 3. Data tables

**Table 2. LA-ICP-MS data for Fe, Si and Ge concentrations and Fe/Si and Ge/Si ratios of Temagami BIF specimens TM1, TM2 and TM3.**

| TM-1 | Fe % | Si % | Ge mg/kg | Fe/Si | Ge/Si*10E6 |
|---|---|---|---|---|---|
| **TM1-M1-1** | 33,4 | 10,1 | 8,00 | 3,30 | 78,8 |
| | 32,7 | 15,7 | 9,21 | 2,09 | 58,7 |
| | 37,1 | 10,5 | 6,87 | 3,53 | 65,3 |
| | 38,9 | 10,5 | 8,69 | 3,69 | 82,4 |
| **TM1-M1-2** | 39,1 | 7,03 | 6,91 | 5,56 | 98,3 |
| | 34,1 | 11,6 | 9,17 | 2,94 | 79,1 |
| | 43,0 | 7,63 | 7,43 | 5,64 | 97,4 |
| | 44,6 | 13,0 | 7,23 | 3,43 | 55,7 |
| **TM1-M1-3** | 43,5 | 7,30 | 7,29 | 5,96 | 99,8 |
| | 22,6 | 22,9 | 6,86 | 0,987 | 30,0 |
| | 59,3 | 3,85 | 15,2 | 15,4 | 393 |
| | 25,0 | 22,2 | 7,53 | 1,12 | 33,9 |
| **TM1-C2-1** | 6,59 | 32,7 | 3,44 | 0,202 | 10,5 |
| | 3,77 | 38,0 | 3,18 | 0,099 | 8,4 |
| | 4,78 | 36,9 | 3,37 | 0,129 | 9,1 |
| | 4,30 | 40,8 | 3,37 | 0,105 | 8,3 |
| **TM1-C2-2** | 3,30 | 35,7 | 2,98 | 0,092 | 8,3 |
| | 20,2 | 23,8 | 3,87 | 0,851 | 16,3 |
| | 8,57 | 34,4 | 3,37 | 0,249 | 9,8 |
| | 10,9 | 37,8 | 3,71 | 0,288 | 9,8 |
| **TM1-M3-1** | 27,6 | 17,5 | 7,86 | 1,580 | 45,0 |
| | 20,8 | 10,5 | 3,13 | 1,98 | 29,7 |
| | 13,1 | 22,3 | 5,05 | 0,589 | 22,7 |
| | 19,2 | 12,5 | 3,61 | 1,54 | 29,0 |
| **TM1-M3-2** | 27,0 | 7,03 | 4,65 | 3,84 | 66,0 |
| | 43,4 | 8,72 | 5,96 | 4,98 | 68,4 |
| | 30,4 | 13,9 | 9,12 | 2,19 | 65,5 |
| | 45,8 | 7,32 | 7,31 | 6,26 | 99,8 |
| **TM1-M3-3** | 55,7 | 3,48 | 7,58 | 16,0 | 217 |
| | 50,8 | 4,42 | 7,44 | 11,5 | 168 |
| | 12,7 | 32,1 | 6,71 | 0,396 | 20,9 |
| | 40,2 | 12,6 | 9,61 | 3,19 | 76,2 |
| | 20,5 | 21,4 | 6,99 | 0,960 | 32,7 |
| **TM1-M3-4** | 19,4 | 18,3 | 4,48 | 1,06 | 24,5 |
| | 3,1 | 34,1 | 3,80 | 0,090 | 11,1 |
| | 17,5 | 21,6 | 3,65 | 0,808 | 16,9 |
| | 7,83 | 48,9 | 5,79 | 0,160 | 11,8 |
| **TM1-M3-5** | 1,86 | 33,2 | 3,05 | 0,056 | 9,2 |
| | 4,80 | 35,8 | 3,71 | 0,134 | 10,4 |
| | 3,70 | 35,3 | 3,65 | 0,105 | 10,3 |
| | 17,3 | 36,4 | 5,25 | 0,476 | 14,4 |
| **TM1-M4-1** | 49,1 | 4,90 | 8,31 | 10,0 | 169 |
| | 33,3 | 6,90 | 7,49 | 4,82 | 109 |
| | 44,2 | 5,79 | 6,20 | 7,64 | 107 |
| | 54,3 | 6,43 | 9,09 | 8,44 | 141 |
| **TM1-M4-2** | 34,0 | 12,0 | 7,46 | 2,84 | 62,4 |
| | 23,9 | 16,1 | 9,30 | 1,48 | 57,7 |
| | 35,1 | 10,8 | 6,88 | 3,25 | 63,7 |
| | 27,4 | 15,2 | 9,00 | 1,80 | 59,1 |
| **TM1-M4-3** | 22,2 | 14,5 | 6,18 | 1,53 | 42,5 |
| | 41,4 | 11,2 | 6,87 | 3,70 | 61,4 |
| | 33,6 | 14,0 | 6,83 | 2,41 | 48,9 |
| | 32,0 | 14,8 | 9,29 | 2,16 | 63,0 |

**Table 2 continued**

| TM-2 | Fe % | Si % | Ge mg/kg | Fe/Si | Ge/Si*10E6 |
|---|---|---|---|---|---|
| **TM-2-M1-1** | 51,6 | 5,73 | 9,75 | 9,01 | 170 |
| | 45,7 | 8,06 | 8,46 | 5,67 | 105 |
| | 49,0 | 8,48 | 8,79 | 5,78 | 104 |
| | 52,4 | 5,98 | 8,37 | 8,75 | 140 |
| **TM-2-M1-2** | 33,5 | 3,90 | 5,85 | 8,59 | 150 |
| | 35,5 | 4,75 | 5,53 | 7,46 | 116 |
| | 55,8 | 6,23 | 9,25 | 8,95 | 148 |
| | 49,7 | 4,07 | 7,85 | 12,2 | 193 |
| **TM-2-C2-1** | 1,16 | 37,8 | 2,61 | 0,0308 | 6,91 |
| | 0,973 | 44,3 | 3,17 | 0,0220 | 7,16 |
| | 0,393 | 43,1 | 3,15 | 0,0091 | 7,31 |
| | 2,05 | 44,8 | 3,51 | 0,0457 | 7,84 |
| **TM-2-C2-2** | 1,58 | 39,7 | 3,03 | 0,0397 | 7,63 |
| | 0,210 | 42,9 | 2,90 | 0,0049 | 6,77 |
| | 2,93 | 48,8 | 4,47 | 0,0601 | 9,17 |
| | 0,575 | 51,0 | 3,47 | 0,0113 | 6,82 |
| **TM-2-M3-1** | 50,7 | 9,18 | 8,92 | 5,52 | 97,2 |
| | 54,5 | 9,18 | 10,3 | 5,94 | 112 |
| | 52,5 | 7,57 | 9,96 | 6,94 | 132 |
| | 58,2 | 7,43 | 11,5 | 7,83 | 155 |
| **TM-2-M3-2** | 53,1 | 7,13 | 7,86 | 7,45 | 110 |
| | 52,7 | 5,37 | 8,76 | 9,82 | 163 |
| | 61,2 | 5,62 | 8,06 | 10,9 | 143 |
| | 56,7 | 8,54 | 8,19 | 6,64 | 95,9 |
| **TM-2-C4-1** | 1,40 | 41,6 | 3,43 | 0,0337 | 8,26 |
| | 1,37 | 46,4 | 3,43 | 0,0296 | 7,39 |
| | 0,703 | 45,9 | 3,74 | 0,0153 | 8,16 |
| | 1,42 | 50,0 | 3,85 | 0,0283 | 7,69 |
| **TM-2-C4-2** | 0,05 | 47,2 | 2,99 | 0,0011 | 6,35 |
| | 2,08 | 44,4 | 3,27 | 0,0468 | 7,36 |
| | 0,775 | 42,3 | 3,08 | 0,0183 | 7,28 |
| | 0,916 | 42,3 | 2,86 | 0,0217 | 6,76 |
| **TM-2-M5-1** | 45,3 | 8,21 | 8,51 | 5,52 | 104 |
| | 48,0 | 5,70 | 7,92 | 8,41 | 139 |
| | 50,6 | 9,67 | 9,44 | 5,23 | 97,6 |
| | 49,3 | 9,31 | 7,19 | 5,29 | 77,3 |
| **TM-2-M5-2** | 51,5 | 7,29 | 8,69 | 7,07 | 119 |
| | 51,4 | 8,20 | 11,0 | 6,27 | 134 |
| | 60,0 | 5,21 | 10,8 | 11,5 | 207 |
| | 51,6 | 9,64 | 9,66 | 5,35 | 100 |
| **TM-2-M5-3** | 46,1 | 8,49 | 6,98 | 5,43 | 82,2 |
| | 43,5 | 10,9 | 9,62 | 3,98 | 88,2 |
| | 56,5 | 6,65 | 10,7 | 8,49 | 160 |
| | 54,2 | 9,08 | 11,1 | 5,96 | 123 |
| **TM-2-C6-1** | 3,53 | 36,2 | 3,52 | 0,0975 | 9,7 |
| | 7,10 | 36,7 | 4,41 | 0,194 | 12,0 |
| | 3,10 | 41,5 | 3,81 | 0,0746 | 9,19 |
| | 10,2 | 41,7 | 4,93 | 0,244 | 11,8 |
| **TM-2-C6-2** | 20,0 | 25,3 | 4,66 | 0,793 | 18,4 |
| | 4,83 | 39,1 | 3,95 | 0,124 | 10,1 |
| | 5,27 | 36,3 | 3,68 | 0,145 | 10,1 |
| | 4,62 | 44,0 | 4,35 | 0,105 | 9,88 |
| **TM-2-M7-2** | 43,2 | 9,79 | 7,55 | 4,41 | 77,2 |
| | 35,3 | 16,6 | 5,86 | 2,13 | 35,4 |
| | 42,3 | 12,2 | 6,62 | 3,46 | 54,1 |
| | 48,5 | 10,8 | 7,87 | 4,50 | 73,1 |
| **TM-2-M7-3** | 45,7 | 8,18 | 7,65 | 5,59 | 93,6 |
| | 46,4 | 9,31 | 7,39 | 4,98 | 79,3 |
| | 48,5 | 8,65 | 8,74 | 5,61 | 101 |
| | 46,8 | 11,3 | 8,24 | 4,13 | 72,7 |

**Table 2 continued**

| TM-3 | Fe % | Si % | Ge mg/kg | Fe/Si | Ge/Si*10E6 |
|---|---|---|---|---|---|
| **TM3-M3-1** | 50,3 | 5,70 | 7,12 | 8,81 | 125 |
| | 47,6 | 6,72 | 8,02 | 7,09 | 119 |
| | 54,1 | 4,73 | 7,47 | 11,4 | 158 |
| | 56,4 | 5,86 | 9,00 | 9,62 | 153 |
| **TM3-M3-2** | 49,9 | 5,20 | 7,33 | 9,59 | 141 |
| | 48,1 | 6,92 | 7,20 | 6,95 | 104 |
| | 42,2 | 9,12 | 6,68 | 4,63 | 73,3 |
| | 54,2 | 5,02 | 7,15 | 10,8 | 142 |
| **TM3-C4-1** | 1,54 | 32,5 | 2,62 | 0,047 | 8,07 |
| | 2,23 | 35,7 | 3,11 | 0,062 | 8,70 |
| | 6,85 | 38,6 | 3,56 | 0,178 | 9,21 |
| | 1,48 | 43,8 | 3,43 | 0,034 | 7,82 |
| **TM3-C4-2** | 1,45 | 35,6 | 2,98 | 0,041 | 8,36 |
| | 6,25 | 33,3 | 3,02 | 0,188 | 9,07 |
| | 5,94 | 35,7 | 3,23 | 0,166 | 9,04 |
| | 1,02 | 42,0 | 3,06 | 0,024 | 7,28 |
| **TM3-M4-1** | 54,4 | 0,657 | 6,38 | 82,9 | 971 |
| | 51,7 | 8,40 | 8,61 | 6,15 | 103 |
| | 53,9 | 6,71 | 7,86 | 8,03 | 117 |
| | 60,0 | 4,47 | 9,72 | 13,4 | 217 |
| **TM3-M4-2** | 45,9 | 8,74 | 8,69 | 5,25 | 99,4 |
| | 51,3 | 4,69 | 8,73 | 10,9 | 186 |
| | 56,8 | 5,27 | 11,0 | 10,8 | 208 |
| | 57,3 | 6,26 | 8,55 | 9,15 | 137 |
| **TM3-M5-1** | 42,4 | 11,3 | 7,06 | 3,76 | 62,5 |
| | 54,1 | 7,19 | 7,22 | 7,52 | 100 |
| | 28,3 | 23,9 | 5,37 | 1,18 | 22,4 |
| | 50,8 | 11,8 | 8,15 | 4,29 | 68,8 |
| **TM3-M5-2** | 40,7 | 13,5 | 7,27 | 3,02 | 54,0 |
| | 44,0 | 9,44 | 6,94 | 4,66 | 73,5 |
| | 43,5 | 13,1 | 7,35 | 3,32 | 56,1 |
| | 56,4 | 8,28 | 9,85 | 6,81 | 118,9 |
| **TM3-M5-3** | 29,6 | 17,5 | 5,52 | 1,69 | 31,6 |
| | 27,5 | 22,4 | 6,29 | 1,23 | 28,1 |
| | 22,8 | 24,6 | 5,10 | 0,928 | 20,8 |
| | 34,0 | 18,0 | 6,63 | 1,89 | 36,8 |
| **TM3-C6-1** | 4,69 | 36,7 | 2,07 | 0,128 | 5,64 |
| | 5,51 | 35,9 | 2,28 | 0,154 | 6,36 |
| | 3,19 | 40,9 | 2,08 | 0,078 | 5,08 |
| | 9,22 | 36,6 | 2,77 | 0,252 | 7,58 |
| **TM3-C6-2** | 4,02 | 33,5 | 1,82 | 0,120 | 5,44 |
| | 4,76 | 36,6 | 2,04 | 0,130 | 5,55 |
| | 5,31 | 38,1 | 2,17 | 0,139 | 5,70 |
| | 4,03 | 37,4 | 2,11 | 0,108 | 5,64 |
| **TM3-C6-3** | 3,34 | 37,6 | 2,40 | 0,089 | 6,39 |
| | 5,41 | 38,9 | 2,89 | 0,139 | 7,45 |
| | 3,51 | 37,8 | 2,43 | 0,093 | 6,44 |
| | 7,20 | 38,5 | 2,83 | 0,187 | 7,36 |
| **TM3-M6-1** | 29,2 | 14,2 | 5,25 | 2,07 | 37,1 |
| | 28,6 | 15,2 | 5,39 | 1,88 | 35,4 |
| | 23,0 | 20,6 | 4,94 | 1,12 | 24,0 |
| | 23,8 | 17,2 | 4,33 | 1,38 | 25,2 |
| **TM3-M6-2** | 24,7 | 17,0 | 4,73 | 1,45 | 27,8 |
| | 31,5 | 15,4 | 4,56 | 2,05 | 29,7 |
| | 20,8 | 21,6 | 4,07 | 0,966 | 18,9 |
| | 36,8 | 14,4 | 6,24 | 2,56 | 43,3 |
| **TM3-M6-3** | 31,6 | 8,33 | 4,72 | 3,80 | 56,7 |
| | 33,1 | 11,7 | 4,71 | 2,82 | 40,1 |
| | 31,4 | 14,6 | 5,23 | 2,14 | 35,8 |
| | 41,4 | 11,1 | 5,86 | 3,73 | 52,7 |
| **TM3-M6-4** | 17,2 | 22,9 | 5,94 | 0,752 | 25,9 |
| | 26,3 | 19,1 | 5,62 | 1,38 | 29,4 |
| | 16,7 | 22,3 | 4,88 | 0,748 | 21,8 |
| | 22,5 | 20,3 | 4,77 | 1,11 | 23,5 |

**Table 3. Concentrations of Fe, Si, Ge and Cr, δ53Cr values, and Th/U ratios of Temagami BIF specimens TM1, TM2 and TM3.**

| Sample | Layer | Type | Fe | Cr | δ53Cr | Th/U | Si* | Fe* | Ge* | Fe/Si* | Ge/Si * 10^6* |
|---|---|---|---|---|---|---|---|---|---|---|---|
| | | | % | mg/kg | ‰ | | % | % | mg/kg | | |
| TM1 | TM1-1 | Fe-band | 40,6 | 3,34 | -0,095 | 2,56 | 10,15 | 33,4 | 7,48 | 3,48 | 79,0 |
| | TM1-2 | chert | 5,05 | 0,33 | 0,235 | 1,38 | 32,7 | 6,59 | 3,37 | 0,166 | 9,5 |
| | TM1-3 | Fe-band | 37,1 | 5,5 | -0,118 | 5,02 | 17,5 | 27,6 | 5,25 | 1,06 | 29,0 |
| | TM1-4 | Fe-band | 36,4 | 5,74 | 0,193 | 3,82 | 4,90 | 49,1 | 7,47 | 3,05 | 62,7 |
| TM2 | TM2-1 | Fe-band | 54,2 | 2,37 | -0,045 | 2,69 | 5,73 | 51,6 | 8,42 | 8,67 | 144 |
| | TM2-2 | chert | 4,16 | 2,61 | -0,06 | 3,36 | 37,8 | 1,16 | 3,16 | 0,0264 | 7,2 |
| | TM2-3 | Fe-band | 56,6 | 6,23 | -0,14 | 2,7 | 9,18 | 50,7 | 8,84 | 7,19 | 122 |
| | TM2-4 | chert | 2,6 | 1,36 | 0,185 | 0,94 | 41,6 | 1,40 | 3,35 | 0,0250 | 7,4 |
| | TM2-5 | Fe-band | 55,5 | 2,36 | -0,12 | 3,31 | 8,21 | 45,3 | 9,53 | 5,74 | 112 |
| | TM2-6a | chert | 4,91 | 0,28 | 0,01 | 0,53 | 36,2 | 3,53 | 4,15 | 0,134 | 10,1 |
| | TM2-6b | chert | | | | | 38,8 | 2,03 | 2,16 | 0,00668 | 4,4 |
| | TM2-7 | Fe-band | | 2,61 | -0,06 | | 9,79 | 43,2 | 7,60 | 4,46 | 75,1 |
| TM3 | TM3-1 | chert | 2,72 | | | 1,15 | | | | | |
| | TM3-2 | Fe-band | 54,1 | | | 3,02 | 5,70 | 50,3 | 7,26 | 9,20 | 133 |
| | TM3-3 | chert | 9,37 | 0,54 | 0,27 | 1,87 | 32,5 | 1,54 | 3,08 | 0,0549 | 8,5 |
| | TM3-4 | Fe-band | 52,4 | 2,67 | -0,115 | 3,35 | 0,657 | 54,4 | 8,65 | 9,97 | 161 |
| | TM3-5 | chert | 6,62 | 0,34 | 0,21 | 0,47 | 13,4 | 36,1 | 7,30 | 4,00 | 67,3 |
| | TM3-6 | Fe-band | 49,2 | 1,64 | -0,06 | 2,37 | 11,3 | 42,4 | 7,00 | 3,17 | 55,0 |
| | TM3-7 | chert | 4,55 | 0,15 | | 0,59 | 36,7 | 4,69 | 2,23 | 0,129 | 6,0 |
| | TM3-8 | Fe-band | 54 | 5,27 | -0,09 | 3,59 | 14,2 | 29,2 | 4,91 | 1,67 | 29,5 |

*mean data obtained by LA-ICP-MS